 CMC, vol.53, no.2, pp.73-89, 2017

The Constitutive Relation of a Fabric Membrane Composite for a Stratospheric Airship Envelope Based on Invariant Theory

Junhui Meng [1,*] and Mingyun Lv [2]

Abstract: The study of stratospheric airships has become the focus in many countries in recent years, because of its potential applications in many fields. Lightweight and high strength envelopes are the keys to the design of stratospheric airships, as it directly determines the endurance flight performance and loading deformation characteristics of the airship. A typical envelope of any stratospheric airship is a coated-fabric material which is composed of a fiber layer and several functional membrane layers. According to composite structure, nonlinearity and viscoelasticity are the two main characteristics of such envelope. Based on the analysis on the interaction between the different components in the micro-mechanical model of the coated-fabric, several invariant values reflecting the characteristics of the envelope material are obtained according to invariant theory. Furthermore, the constitutive equation that describes the viscoelasticity of the envelope material is derived. The constitutive equation can represent both the individual roles of the warp and weft fibers, and their further coupled interactions. The theoretical computation results were verified by off-axial tension tests. The results can help gain a deeper understanding of the mechanical mechanism and provide a reference for structural design of envelope material.

Keywords: Stratospheric airship, fabric membrane composite, constitutive relation, invariant theory, viscoelasticity.

1 Introduction

The stratospheric layer, at a height of 10km~30km, is a new strategic space, which is suitable for the large-scale airships. Warmer upper layers and cooler lower layers makes the stratosphere dynamically stable: there is no regular convection and associated turbulence in this part of the atmosphere, and the statistics indicate that there is a lull in

[1] College of Engineering, China Agricultural University, Beijing 100083, PR China.

[2] School of Aeronautic Science and Engineering, Beihang University, Beijing 100191, PR China.

* Corresponding Author: Lecturer, +86-010 -82318116.

E-mail: mengjh@cau.edu.cn (Junhui Meng).

the wind between 20km and 22km on a yearly average [Roney (2007)]. Over the years, engineers and scientists devoted great efforts to developing various platforms which can operate at this altitude beyond traditional aircraft maneuvers, since these platforms could provide a vantage point for scientific exploration as well as allows for better communication and real-time surveillance than satellites[Zheng et al. (2014); Zheng and Huo. (2013)]. As a lighter-than-air vehicle, stratospheric airships (SSA) have the ability of fixing a position for a long-time operation and performs obvious advantages in payload capacity. Therefore, airships have become a typical stratospheric platform that many countries are competing to develop. Advanced projects related to SSAs have already provided interesting achievements in several groups, such as High-Altitude Airship of Lockheed Martin Company[Jamison et al. (2005)], Stratospheric Airship Program of South Korea[Lee et al. (2006)], Hisentinel Airship of Southwest Research Institute of the United States[Smith and Rainwater (2003)] and Stratospheric Platform Airship of Japan[Inamoto et al. (2003)]. Some of these airships are on the flight test stage and are expected to realize practical applications in the near future.

The envelope is major part of airship structures, which is used to contain lifting gas and maintain aerodynamic configuration. Because of the complex working condition and stratospheric environment, many kinds of materials with a single component cannot satisfy all requirements. The typical envelope of the SSA is woven fabric which is coated and laminated together with high-modulus film and adhesives by optimizing process parameters[Khoury (2012)]. As the main load-bearing structure, the fabric layer is always woven by synthetic fabric materials such as Vectran, Mylar, PBO and so on. The functional membrane layers are laminated by different layers according to the need of UV and ozone protection, helium retention and thermal insulation. Polyvinyl fluoride film(Tedlar) and Polyvinylidene Fluoride (PVDF) are appropriate choices. The laminated membranes must be sewn and cemented together or heated-sealed to make a large gas-holding envelope.

According to the structure of the envelope material for the SSA, it can be described as a kind of flexible fabric membrane composite, which is the same as low altitude airship envelope material[Yousef, Stylios (2014)] and the ground architectural membrane structure[Chen et al. (2008); Yingying et al. (2014); Ambroziak, Kłosowski (2014)]. To describe its mechanical properties, the fabric membrane material can be regarded as elastic, nonlinear-elastic[Ambroziak (2005)], viscoelastic[Argyris, Doltsinis (1991)] or viscoplastic [Kłosowski et al. (2004)] in many analysis models.

In the last decades, a great deal of research effort has been devoted to the development of the constitutive theory of fiber-reinforced composites. As an anisotropic material, the

fabric composite belongs to a very important class of materials which are employed frequently in a variety of industrial applications. Nayfeh and Kress (1997) developed a non-linear constitutive model for plain-weave composites which was based on the micromechanical behavior of a representative unit cell. The global constitutive relationships were consistently derived from the total strain energy of the system. Compatibility of the constituent's geometric non-linearities was fully taken into account in their paper where the matrix played the role of an elastic foundation and was thus modeled as a continuum. Nedjar (2007) presented a fully three-dimensional constitutive model for anisotropic viscoelasticity suitable for the macroscopic description of fibre reinforced composites that experience finite strains. An essential feature of the model was that the matrix and the fibres were treated separately allowing then as many bundles of fibres as desired. Moreover, the relaxation and/or creep response was based on the multiplicative viscoelastic split of the deformation gradient combined with the assumption of viscoelastic potentials for each compound. By using the stress energy density referring to the deformed volume, Luo and Chou (1988) derived a nonlinear constitutive model for flexible composites composed of aligned continuous fibers rather than woven fibers in an elastomeric matrix under finite deformation. The theoretical derivation was based upon the Eulerian description to account for the material non-linearity including stretch-shear coupling. The fiber orientation was obtained from strains in their model through an iterative calculation. Jiang et al (2000) presented a stress and strain averaging procedure in their paper for local/global analysis of plain-weave fabric composites. Within a representative volume cell, using uniform stress and uniform strain assumptions, the constitutive equations were averaged along the thickness direction. The cell was then divided into many sub-cells and an averaging was performed again by assuming uniform stress distribution in each sub-cell to obtain the effective stress/strain relations of the sub-cell. In addition, the papers by Kyriacou et al. (1996); Weiss et al. (1996); Bonet and Burton (1998) describe constitutive equations for fiber oriented hyperelastic materials in the nonlinear stress and deformation domain and provide computational aspects for their finite element implementation. But the envelope material of the SSA is quite different with them in several aspects. Much higher strength-to-weight ratio is needed for the SSA envelope, and the working environment is also more severe because of ultraviolet aging, ozone oxidation and high-low cyclic temperatures. A valid and widely applicable model to investigate the constitutive relation of the envelope material for the SSA needs to be developed.

The purpose of this paper is to investigate the constitutive relation of the envelope material for the SSA. The framework of this paper is provided to illustrate the main processing flow, as shown in Fig. 1. Firstly, the mesoscopic mechanism of interaction

between yarns and resin matrix of the envelope material are studied based on the moment equilibrium. According to invariant theory, the system energy can be expressed by several invariants, which can be transformed by different variables. Therefore, the constitutive equation, including viscosity and elasticity of fiber and matrix and directional properties of yarns, can be derived and simplified by the on-axial and off-axial tensile tests. It is hoped that this investigation could provide a better understanding on the mechanical characteristics of the envelope material, which is instructional to the structural design of the SSA.

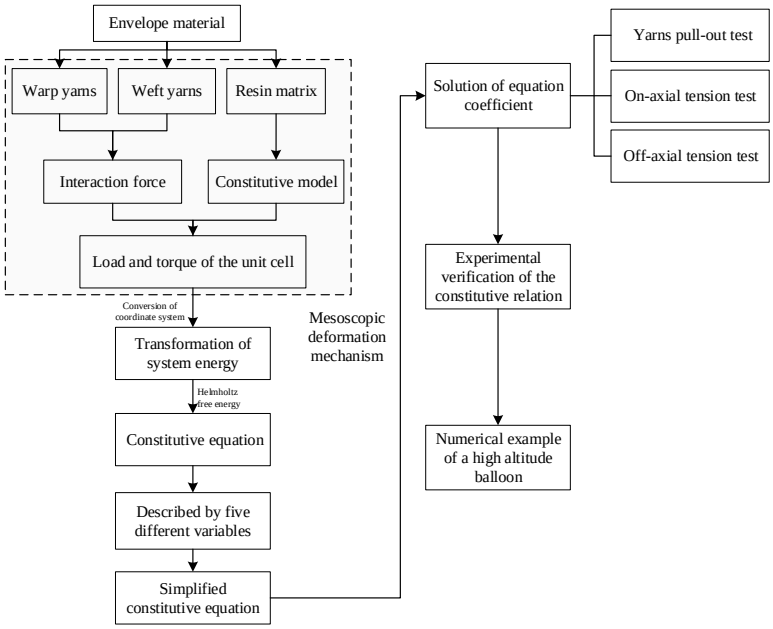

Figure 1: The main processing flow of this paper

2 Mesoscopic deformation mechanism

The most crucial difference between textile and fabric composite material is the existence of resin matrix, which hinders the interaction between warp and weft yarns in the fabric composite. To explore the constitutive relation of the envelope material, the deformation mechanism based on mesoscopic model should first be investigated. The deformation of envelope material under shear load is observed by a scanning electron microscope (SEM), which is shown in Fig. 2. It can be seen from the figure that warp and weft yarns skews from the orthogonal with the increase of deformation. There are two obvious phases of the envelope material shear deformation. The resin matrix among yarns is extruded first because of its lower modulus. In this stage, the external force is balanced by resistance of resin matrix and friction between orthotropic yarns. Subsequently, the

yarns are pulled straight, and oblique angle becomes a fixed value, which is called locking angle. After that, extrusion force is added to resist the external force and the shear deformation comes into the second phase.

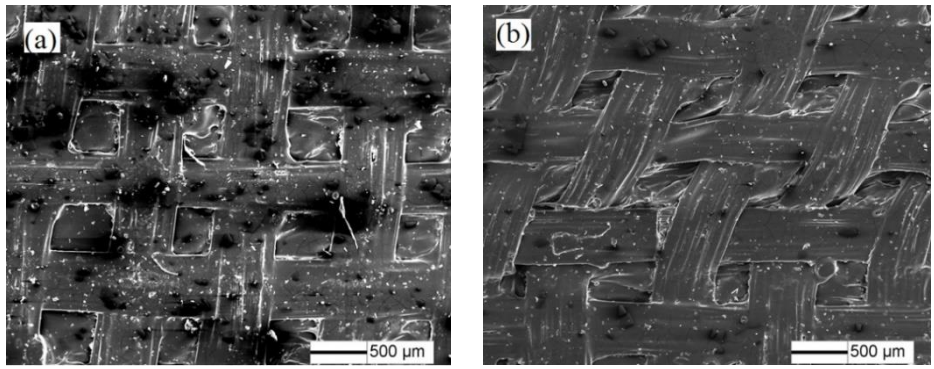

Figure 2: The SEM observation of envelope material deformation

The relation between warp and weft yarns before and after locking angle stage is shown in Fig. 3. The Unit Cell is indicated as the shaded area. The diameter and interval of yarns are assumed as d_0 and g_0, respectively. So, the width of a unit cell is

$$S = d_0 + g_0 \tag{1}$$

When the adjacent yarns contact just now, the diameter of each yarn is still $d = d_0$. The shear locking angle can be derived as follows:

$$\gamma_L = \cos^{-1}\left(\frac{d_0}{S}\right) \tag{2}$$

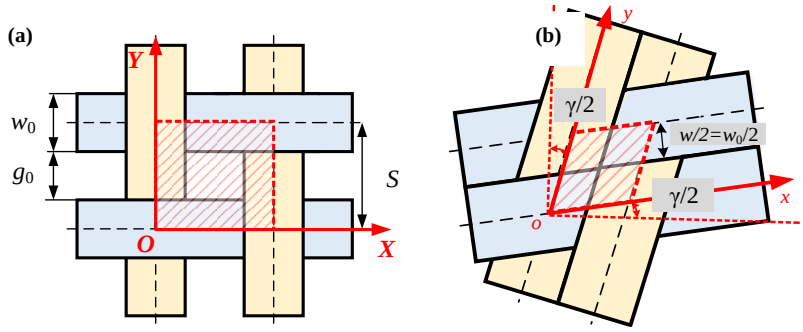

Figure 3: The relation between warp and weft yarns at (a) nondeformed stage and (b) locking angle stage

With the continue of shear action, the adjacent yarns squeeze each other, and the diameter of each yarn is

$$d = S\cos\gamma \tag{3}$$

Consequently, the diameter of each yarn under any conditions can be described as follows:

$$d = \begin{cases} d_0 & \gamma \le \gamma_L \\ S\cos\gamma & \gamma > \gamma_L \end{cases} \tag{4}$$

The resin matrix can be regarded as isotropic material, whose constitutive model can be expressed as

$$\sigma_{ij} = -p\delta_{ij} + 2\eta D_{ij} \tag{5}$$

Where, p is the hydrostatic pressure, η is the viscosity coefficient, D is the deformation rate tensor. So, the shear load can be expressed as follows:

$$\sigma_{12} = 2\eta D_{12} \tag{6}$$

The torque of shear load about the center of unit cell can be obtained as follows:

$$M_R = \sigma_{12} S^2 t\cos\gamma = 2\eta D_{12} S^2 t\cos\gamma \tag{7}$$

Where, t is the thickness of the unit cell. And because $D_{12} = -\dot{\gamma}\tan\gamma$, Equation (7) can be transformed into as follows:

$$M_R = -2\eta\dot{\gamma} S^2 t\sin\gamma \tag{8}$$

After locking angle, the extrusion force on the unit cell is shown in Fig. 4. The lateral distribution extrusion force is expressed as F_c, so the torque of extrusion force can be indicated as

$$M_c = 2\int_{(\sin\gamma-1)S/2}^{(1+\sin\gamma)S/2} F_c x dx = S^2 F_c \sin\gamma \tag{9}$$

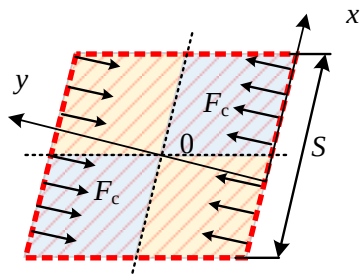

Figure 4: Extrusion force on the unit cell after locking angle

Friction acted between orthogonal yarns before and after the locking angle. The frictional coefficient can be derived from a single fiber pull-out test. The detailed test methods can be obtained from reference [Meng et al. (2016)]. And the torque of friction load about

the center of unit cell can be obtained as follows.

$$M_F = \frac{1}{6}\mu\pi dF\int_0^{\frac{\pi}{2}} \frac{d\varphi}{\cos^3(\theta-\varphi)}\cos\gamma \tag{10}$$

Where, μ is the frictional coefficient, θ is the angle between warp and weft yarns, F is the axial force along the yarn direction.

3 Macroscopic constitutive relation

3.1 Analysis of the system energy

As shown in Fig. 2(a), in the original state, when there is no deformation, the warp yarns perpendicular to the weft yarns, which is signified as the Lagrange coordinate system *OXY*. While the warp and weft yarns become oblique from orthotropic after deformation, the Euler coordinate system *oxy* is used to express it, as shown in Fig. 2(b). Under the Lagrange coordinate system, unit vectors $\mathbf{Q}$ and $\mathbf{P}$ are regarded as the directions of warp and weft yarns, respectively. Correspondingly, unit vectors $\mathbf{q}$ and $\mathbf{r}$ represent the directions of warp and weft yarns under the Euler coordinate system, respectively. The structure tensors under the *OXY* coordinates are $\mathbf{M}=\mathbf{Q}\otimes\mathbf{Q}$, $\mathbf{N}=\mathbf{R}\otimes\mathbf{R}$, $\mathbf{P}=\mathbf{Q}\otimes\mathbf{R}$, $\mathbf{P}^{\mathrm{T}}=\mathbf{R}\otimes\mathbf{Q}$, and under the *oxy* coordinates, $\mathbf{m}=\mathbf{q}\otimes\mathbf{q}$, $\mathbf{n}=\mathbf{r}\otimes\mathbf{r}$, $\mathbf{p}=\mathbf{q}\otimes\mathbf{r}$ $\mathbf{p}^{\mathrm{T}}=\mathbf{r}\otimes\mathbf{q}$.

Under the isothermal condition, the second law of thermodynamics can be represented as the inequation of Clausius-Duhem:

$$\boldsymbol{\Omega}=\mathbf{S}:\dot{\mathbf{C}}/2-\dot{\boldsymbol{\Psi}}\geq 0 \tag{11}$$

where, $\boldsymbol{\Omega}$ is the entropy generation, $\mathbf{S}$ is the second Piola-Kirchhoff stress tensor, $\mathbf{C}$ is the right Cauchy-Kirchhoff deformation tensor, $\boldsymbol{\Psi}$ is the Helmholtz free energy function and can be expressed by the following five different variables:

$$\boldsymbol{\Psi}=\boldsymbol{\Psi}\left(\mathbf{C},\dot{\mathbf{C}},\mathbf{M},\mathbf{N},\mathbf{P}\right) \tag{12}$$

where, $\mathbf{C}$ expresses the elastic property of fibers in the envelope material, $\dot{\mathbf{C}}$ indicates the viscosity of resin matrix, and the last three variables $\mathbf{M}$, $\mathbf{N}$, $\mathbf{P}$ denote the directional properties of fibers in the envelope material. Substituting equation (12) into (11), the entropy generation can be transformed as follows.

$$\boldsymbol{\Omega} = \left(\mathbf{S} - 2\partial\boldsymbol{\Psi}/\partial\mathbf{C}\right) : \dot{\mathbf{C}}/2 \geq 0 \tag{13}$$

When it is under the critical condition, the equation can be derived as $\mathbf{S} - 2\partial\boldsymbol{\Psi}/\partial\mathbf{C} = 0$, i.e.

$$\mathbf{S} = 2\frac{\partial\boldsymbol{\Psi}\left(\mathbf{C}, \dot{\mathbf{C}}, \mathbf{M}, \mathbf{N}, \mathbf{P}\right)}{\partial\mathbf{C}} \tag{14}$$

It can be seen from equation (14) that the constitutive equation can be derived once the Helmholtz free energy is provided. The Helmholtz free-energy can be regarded as a function composed of several invariants transformed by five different variables. The constitutive equation will be derived in the next section based on invariant theory.

3.2 Constitutive equation based on the invariant theory

According to invariant theory, Holzapfel and Gasser [Holzapfel, Gasser (2001)] put forward that the Helmholtz free-energy function $\boldsymbol{\Psi}$ of the elastic material can be signified by seven different invariants. Similarly, the Helmholtz free-energy function $\boldsymbol{\Psi}$ of the envelope material also can be expressed by several invariants, which can be transformed by five different variables $\mathbf{C}$, $\dot{\mathbf{C}}$ $\mathbf{M}$, $\mathbf{N}$ and $\mathbf{P}$. The invariants are shown as follows.

$$\begin{aligned}
&I_1 = tr\mathbf{C}, I_2 = tr\mathbf{C}^2, I_3 = tr\dot{\mathbf{C}}, I_4 = tr\dot{\mathbf{C}}^2,\\
&I_5 = tr\mathbf{C}\otimes\mathbf{M}, I_6 = tr\mathbf{C}\otimes\mathbf{N}, I_7 = tr\mathbf{C}\otimes\mathbf{P},\\
&I_8 = tr\dot{\mathbf{C}}\otimes\mathbf{M}, I_9 = tr\dot{\mathbf{C}}\otimes\mathbf{N}, I_{10} = tr\dot{\mathbf{C}}\otimes\mathbf{P},\\
&I_{11} = tr\mathbf{C}^2\otimes\mathbf{M}, I_{12} = tr\mathbf{C}^2\otimes\mathbf{N}, I_{13} = tr\mathbf{C}^2\otimes\mathbf{P},\\
&I_{14} = tr\dot{\mathbf{C}}^2\otimes\mathbf{M}, I_{15} = tr\dot{\mathbf{C}}^2\otimes\mathbf{N}, I_{16} = tr\dot{\mathbf{C}}^2\otimes\mathbf{P},\\
&I_{17} = tr\mathbf{C}\dot{\mathbf{C}}\otimes\mathbf{M}, I_{18} = tr\mathbf{C}\dot{\mathbf{C}}\otimes\mathbf{N}, I_{19} = tr\mathbf{C}\dot{\mathbf{C}}\otimes\mathbf{P},\\
&I_{20} = tr\mathbf{C}^2\dot{\mathbf{C}}\otimes\mathbf{M}, I_{21} = tr\mathbf{C}^2\dot{\mathbf{C}}\otimes\mathbf{N}, I_{22} = tr\mathbf{C}^2\dot{\mathbf{C}}\otimes\mathbf{P},\\
&I_{23} = tr\mathbf{C}\dot{\mathbf{C}}^2\otimes\mathbf{M}, I_{24} = tr\mathbf{C}\dot{\mathbf{C}}^2\otimes\mathbf{N}, I_{25} = tr\mathbf{C}\dot{\mathbf{C}}^2\otimes\mathbf{P},\\
&I_{26} = tr\mathbf{C}^2\dot{\mathbf{C}}^2\otimes\mathbf{M}, I_{27} = tr\mathbf{C}^2\dot{\mathbf{C}}^2\otimes\mathbf{N}, I_{28} = tr\mathbf{C}^2\dot{\mathbf{C}}^2\otimes\mathbf{P}
\end{aligned} \tag{15}$$

Where, the invariants containing $\mathbf{C}$ and $\dot{\mathbf{C}}$ indicate the intrinsic properties of fiber and matrix, invariants containing $\mathbf{M}$, $\mathbf{N}$ and $\mathbf{P}$ represent both directional properties of fiber and the material intrinsic properties. Therefore, the Helmholtz free-energy function $\boldsymbol{\Psi}$ can be written as $\boldsymbol{\Psi} = \boldsymbol{\Psi}\left(I_1, \cdots, I_{28}\right)$, and the constitutive equation can be translated into

$$\mathbf{S} = 2\frac{\partial \boldsymbol{\Psi}\left(I_1, \quad \cdots, \quad I_{28}\right)}{\partial I_r}\frac{\partial I_r}{\partial \mathbf{C}} \tag{16}$$

where, $\mathbf{S}$ is the second Piola-Kirchhoff stress and $\mathbf{C}$ is the right Cauchy-Green deformation tensor. The concrete form of the constitutive equation is as follows.

$$\begin{aligned}
\mathbf{S} = & -p\mathbf{I} + \eta_1\mathbf{C} + \eta_2\dot{\mathbf{C}} + \eta_3\dot{\mathbf{C}}^2 + \eta_4\left(\mathbf{C}\dot{\mathbf{C}} + \dot{\mathbf{C}}\mathbf{C}\right) + \eta_5\left(\mathbf{C}\dot{\mathbf{C}}^2 + \dot{\mathbf{C}}^2\mathbf{C}\right) \\
& + \eta_6\mathbf{M} + \eta_7\mathbf{N} + \eta_8\left(\mathbf{M}\dot{\mathbf{C}} + \dot{\mathbf{C}}\mathbf{M}\right) + \eta_9\left(\mathbf{N}\dot{\mathbf{C}} + \dot{\mathbf{C}}\mathbf{N}\right) \\
& + \eta_{10}\left(\mathbf{P}\dot{\mathbf{C}} + \dot{\mathbf{C}}\mathbf{P} + \mathbf{P}^{\mathrm{T}}\dot{\mathbf{C}} + \dot{\mathbf{C}}\mathbf{P}^{\mathrm{T}}\right) + \eta_{11}\left(\mathbf{MC} + \mathbf{CM}\right) + \eta_{12}\left(\mathbf{NC} + \mathbf{CN}\right) \\
& + \eta_{13}\left(\mathbf{PC} + \mathbf{CP} + \mathbf{P}^{\mathrm{T}}\mathbf{C} + \mathbf{CP}^{\mathrm{T}}\right) + \eta_{14}\left(\mathbf{M}\dot{\mathbf{C}}^2 + \dot{\mathbf{C}}^2\mathbf{M}\right) + \eta_{15}\left(\mathbf{N}\dot{\mathbf{C}}^2 + \dot{\mathbf{C}}^2\mathbf{N}\right) \\
& + \eta_{16}\left(\mathbf{P}\dot{\mathbf{C}}^2 + \dot{\mathbf{C}}^2\mathbf{P} + \mathbf{P}^{\mathrm{T}}\dot{\mathbf{C}}^2 + \dot{\mathbf{C}}^2\mathbf{P}^{\mathrm{T}}\right) + \eta_{17}\left(\mathbf{MC}\dot{\mathbf{C}} + \mathbf{C}\dot{\mathbf{C}}\mathbf{M}\right) \\
& + \eta_{18}\left(\mathbf{NC}\dot{\mathbf{C}} + \mathbf{C}\dot{\mathbf{C}}\mathbf{N}\right) + \eta_{19}\left(\mathbf{PC}\dot{\mathbf{C}} + \mathbf{C}\dot{\mathbf{C}}\mathbf{P} + \mathbf{P}^{\mathrm{T}}\mathbf{C}\dot{\mathbf{C}} + \mathbf{C}\dot{\mathbf{C}}\mathbf{P}^{\mathrm{T}}\right) \\
& + \eta_{20}\left(\mathbf{MC}\dot{\mathbf{C}}^2 + \mathbf{C}\dot{\mathbf{C}}^2\mathbf{M}\right) + \eta_{21}\left(\mathbf{NC}\dot{\mathbf{C}}^2 + \mathbf{C}\dot{\mathbf{C}}^2\mathbf{N}\right) \\
& + \eta_{22}\left(\mathbf{PC}\dot{\mathbf{C}}^2 + \mathbf{C}\dot{\mathbf{C}}^2\mathbf{P} + \mathbf{P}^{\mathrm{T}}\mathbf{C}\dot{\mathbf{C}}^2 + \mathbf{C}\dot{\mathbf{C}}^2\mathbf{P}^{\mathrm{T}}\right)
\end{aligned} \tag{17}$$

Where, $\eta_i\left(i = 1, \cdots, 22\right)$ is the coefficient which can be derived by mechanics tests.

3.3 Simplification of the constitutive equation

Equation (17) is the common form of constitutive relation for the fabric composite material, which can be simplified according to the mechanical properties of envelope material. Considering the symmetry between warp and weft direction of the envelope material, the following equations can be derived:

$$\eta_6 = \eta_7, \eta_8 = \eta_9, \eta_{11} = \eta_{12}, \eta_{14} = \eta_{15}, \eta_{17} = \eta_{18}, \eta_{20} = \eta_{21} \tag{18}$$

Wherein, η_6 and η_7 indicate the tension in the direction of $\mathbf{M}$ and $\mathbf{N}$. Their magnitudes are equal, but the direction is not the same, which are represented by T_q and T_r, respectively. In addition, to maintain the continuity of the coefficients, the symbols can be re-expressed as the following forms:

$$\begin{aligned}
&\eta_i = \eta_i^{'}\left(i = 1, \cdots, 5\right), \eta_8 = \eta_6^{'}, \eta_{10} = \eta_7^{'}, \eta_{11} = \eta_8^{'}, \eta_{13} = \eta_9^{'}, \\
&\eta_{14} = \eta_{10}^{'}, \eta_{16} = \eta_{11}^{'}, \eta_{17} = \eta_{12}^{'}, \eta_{19} = \eta_{13}^{'}, \eta_{20} = \eta_{14}^{'}, \eta_{22} = \eta_{15}^{'}
\end{aligned} \tag{19}$$

Substituting equation (18) and (19) into (17), the simplified constitutive equation can be obtained as follows:

$$\begin{aligned}\mathbf{S} = & -p\mathbf{I} + \mathbf{T}_q\mathbf{M} + \mathbf{T}_r\mathbf{N} + \eta_1'\dot{\mathbf{C}} + \eta_2'\dot{\mathbf{C}} + \eta_3'\dot{\mathbf{C}}^2 + \eta_4'\left(\mathbf{C}\dot{\mathbf{C}} + \dot{\mathbf{C}}\mathbf{C}\right) + \eta_5'\left(\mathbf{C}\dot{\mathbf{C}}^2 + \dot{\mathbf{C}}^2\mathbf{C}\right) \\ & + \eta_6'\left(\mathbf{M}\dot{\mathbf{C}} + \dot{\mathbf{C}}\mathbf{M} + \mathbf{N}\dot{\mathbf{C}} + \dot{\mathbf{C}}\mathbf{N}\right) + \eta_7'\left(\mathbf{P}\dot{\mathbf{C}} + \dot{\mathbf{C}}\mathbf{P} + \mathbf{P}^{\mathrm{T}}\dot{\mathbf{C}} + \dot{\mathbf{C}}\mathbf{P}^{\mathrm{T}}\right) \\ & + \eta_8'\left(\mathbf{MC} + \mathbf{CM} + \mathbf{NC} + \mathbf{CN}\right) + \eta_9'\left(\mathbf{PC} + \mathbf{CP} + \mathbf{P}^{\mathrm{T}}\mathbf{C} + \mathbf{CP}^{\mathrm{T}}\right) \\ & + \eta_{10}'\left(\mathbf{M}\dot{\mathbf{C}}^2 + \dot{\mathbf{C}}^2\mathbf{M} + \mathbf{N}\dot{\mathbf{C}}^2 + \dot{\mathbf{C}}^2\mathbf{N}\right) + \eta_{11}'\left(\mathbf{P}\dot{\mathbf{C}}^2 + \dot{\mathbf{C}}^2\mathbf{P} + \mathbf{P}^{\mathrm{T}}\dot{\mathbf{C}}^2 + \dot{\mathbf{C}}^2\mathbf{P}^{\mathrm{T}}\right) \\ & + \eta_{12}'\left(\mathbf{MC}\dot{\mathbf{C}} + \mathbf{C}\dot{\mathbf{C}}\mathbf{M} + \mathbf{NC}\dot{\mathbf{C}} + \mathbf{C}\dot{\mathbf{C}}\mathbf{N}\right) + \eta_{13}'\left(\mathbf{PC}\dot{\mathbf{C}} + \mathbf{C}\dot{\mathbf{C}}\mathbf{P} + \mathbf{P}^{\mathrm{T}}\mathbf{C}\dot{\mathbf{C}} + \mathbf{C}\dot{\mathbf{C}}\mathbf{P}^{\mathrm{T}}\right) \\ & + \eta_{14}'\left(\mathbf{MC}\dot{\mathbf{C}}^2 + \mathbf{C}\dot{\mathbf{C}}^2\mathbf{M} + \mathbf{NC}\dot{\mathbf{C}}^2 + \mathbf{C}\dot{\mathbf{C}}^2\mathbf{N}\right) + \eta_{15}'\left(\mathbf{PC}\dot{\mathbf{C}}^2 + \mathbf{C}\dot{\mathbf{C}}^2\mathbf{P} + \mathbf{P}^{\mathrm{T}}\mathbf{C}\dot{\mathbf{C}}^2 + \mathbf{C}\dot{\mathbf{C}}^2\mathbf{P}^{\mathrm{T}}\right)\end{aligned} \tag{20}$$

In the current configuration, the constitutive relation can be expressed by Cauchy stress $\boldsymbol{\sigma}$, left Cauchy-Green deformation tensor $\mathbf{B}$ and deformation rate tensor $\mathbf{D}$. According to the relationship of original configuration and current configuration, the following equations can be derived:

$$\mathbf{S} = \mathbf{F}^{-1}\boldsymbol{\sigma}\mathbf{F}^{-\mathrm{T}} \tag{21}$$

$$\mathbf{B} = \left(\mathbf{F}^{\mathrm{T}}\right)^{-1}\mathbf{C}\mathbf{F}^{\mathrm{T}} \tag{22}$$

$$\frac{1}{2}\dot{\mathbf{C}} = \mathbf{F}^{T}\mathbf{D}\mathbf{F} \tag{23}$$

It is assumed that fibers of the envelope material cannot be elongated. After unifying all the coefficients, the constitutive equation in the current configuration can be obtained as follows:

$$\begin{aligned}\boldsymbol{\sigma} = & -p\mathbf{I} + \mathbf{T}_q\mathbf{m} + \mathbf{T}_r\mathbf{n} + \alpha_1\mathbf{D} + \alpha_2\mathbf{D}^2 \\ & + \alpha_3\left(\mathbf{mD} + \mathbf{Dm} + \mathbf{nD} + \mathbf{Dn}\right) + \alpha_4\left(\mathbf{pD} + \mathbf{Dp} + \mathbf{p}^{\mathrm{T}}\mathbf{D} + \mathbf{Dp}^{\mathrm{T}}\right) \\ & + \alpha_5\left(\mathbf{mD}^2 + \mathbf{D}^2\mathbf{m} + \mathbf{nD}^2 + \mathbf{D}^2\mathbf{n}\right) + \alpha_6\left(\mathbf{pD}^2 + \mathbf{D}^2\mathbf{p} + \mathbf{p}^{\mathrm{T}}\mathbf{D}^2 + \mathbf{D}^2\mathbf{p}^{\mathrm{T}}\right)\end{aligned} \tag{24}$$

4 Experimental verification of the constitutive relation

The constitutive equation of the envelope material is derived in last section. There are six different coefficients $\alpha_i\left(i = 1, \cdots, 6\right)$ in the equation with different signification. α_1 and α_2 represent mechanical properties of resin matrix, which can be derived by the fiber pull-out experiment. While α_3 and α_5 indicate the mechanical properties of warp and weft yarns, which can be derived by the on-axial tension test. α_4 and α_6 denote interaction of warp and weft yarns, which can be obtained by the off-axial tension test.

The uniaxial tension tests are carried out to get the mechanical properties of the envelope material with off-axial angles of θ=0° and θ=45°. The uniaxial tensile test equipment is a WDW-100 machine, shown in Fig. 5(a). As shown in the figure, the specimen for the

uniaxial tension test is tailored to be a strip which refers to the standard of ASTM D1004-09. Effective length and the width of the specimen are 200 ± 1mm and 50 ± 0.5mm, and the clamped lengths in two sides of the specimens are $20\text{mm} \pm 0.5$mm, respectively. All the specimens are loaded by equal displacement mode with the speed of 5 mm/min. The real-time data of load and displacement are recorded by sensors clamped in the two ends of the specimens. The static tensile curves are shown in a microcomputer and the test performed at room temperature of 25 ℃ and in the relative humidity of 50% RH.

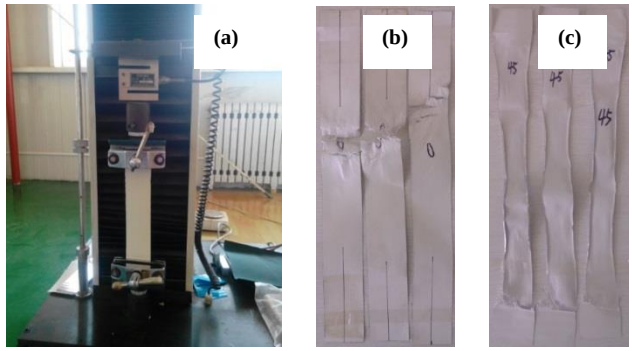

Figure 5: (a) The uniaxial tensile test machine (b) on-axial specimens and (c) off-axial specimens

The macroscopic damage morphologies of specimens of on-axial specimens and off-axial specimens are shown in Fig. 5(b) and (c). As shown in the figures, all the off-axial specimens are cut off from one side, which are differ from on-axial specimens. The probable reason is that the shear force between fabric and adhesive matrix is passed to the end of the specimen until the fibers are broken one by one, rather than fracture simultaneously. It also can be drawn that the stress concentration effects only happen in the scope of local crack area without wide range of yield for on-axial specimens. The on-axial specimens are snapped from the central positions and the warp and weft fibers are cut off along the vertical direction of the tensile stress axial line at the same time.

As for the off-axial tensile test, the relationship of displacement δ and shear angle γ can be derived as follows.

$$\begin{cases} \cos\theta = \dfrac{\delta}{2L} + \cos\left(\dfrac{\pi}{4}\right) \\ \gamma = \dfrac{\pi}{2} - 2\theta \end{cases} \tag{25}$$

The initial direction of warp and weft yarns are $\mathbf{Q} = (1 \quad 0 \quad 0)$ and $\mathbf{R} = (0 \quad 1 \quad 0)$,

respectively. After tensile deformation, two directions of the yarns become to $\mathbf{q}=\left(\cos\frac{\gamma}{2}\quad \sin\frac{\gamma}{2}\quad 0\right)$,and $\mathbf{r}=\left(\sin\frac{\gamma}{2}\quad \cos\frac{\gamma}{2}\quad 0\right)$. Meanwhile, according to the relationship of Lagrange coordinates and Euler coordinates, deformation gradient tensor $\mathbf{F}_{ij}$, left Cauchy-Green deformation tensor $\mathbf{B}_{ij}$ and deformation rate tensor $\mathbf{D}_{ij}$ can be calculated as follows:

$$\mathbf{F}_{ij}=\begin{bmatrix} \dfrac{\cos\frac{\gamma}{2}}{\cos\gamma} & -\dfrac{\sin\frac{\gamma}{2}}{\cos\gamma} & 0 \\ -\dfrac{\sin\frac{\gamma}{2}}{\cos\gamma} & \dfrac{\cos\frac{\gamma}{2}}{\cos\gamma} & 0 \\ 0 & 0 & \cos\gamma \end{bmatrix} \tag{26}$$

$$\mathbf{B}_{ij}=\begin{bmatrix} 1+\tan^2\gamma & -\tan\gamma\sec\gamma & 0 \\ -\tan\gamma\sec\gamma & \sec^2\gamma & 0 \\ 0 & 0 & 1 \end{bmatrix} \tag{27}$$

$$\mathbf{D}_{ij}=\frac{\dot{\gamma}}{2}\begin{bmatrix} \tan\gamma & -\sec\gamma & 0 \\ -\sec\gamma & \tan\gamma & 0 \\ 0 & 0 & -2\tan\gamma \end{bmatrix} \tag{28}$$

According to the above equations and the tensile tests, the constitutive relation can be derived from equation (24). And the comparison of tensile tests with the off-axial angle of θ=45° specimen and the numerical results is shown in Fig. 6. It can be seen from the figure that there are two obvious stages for the stress-strain curves. In the first stage, warp yarns and weft yarns interact with each other and become from orthogonality to oblique until the intersection angle to locking angle. The locking angle occurs when the strain is 2.3% and after that the intersection angle remains unchanged. Note that theoretical and experimental curves yield a good correspondence with deviations below the strain of 4.5% and above the strain of 28.5%. Therefore, the theoretical model is an acceptable model to the engineering applications. Besides, analyzing the plausible reason of deviations, the interaction of yarns and matrix is not homogeneous before the locking angle and the yarns become elongated near damage which is not identical with the assumption.

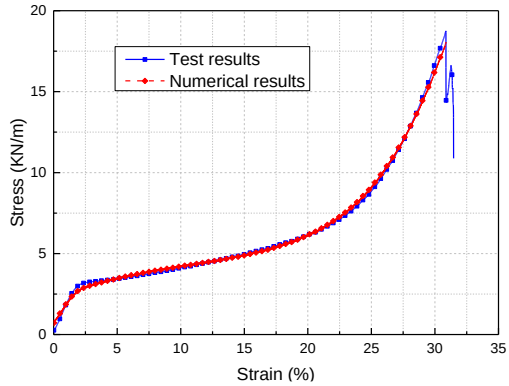

Figure 6: Comparison of test results and numerical results

5 Numerical example of a high-altitude balloon

In the traditional engineering model, the envelope material of airship is regarded as isotropic for simplification. The immediate consequence it brings about is that the safety factor should be a large value, which is a waste of envelope material. The proposed constitutive relation in this paper can reflect mechanical properties of the envelope material accurately. In this section, the numerical simulation of a high-altitude balloon flight at stratosphere with a diameter of 40m is carried out to apply the proposed constitutive relation. The finite element model (FEM) of the altitude balloon is developed at first. A user defined material subroutine (UMAT) is written to apply the proposed constitutive relation into the FEM and the simulation is achieved in ABAQUS/Standard.

The wind resistance ability of the high-altitude balloon on the ground before launching is an important design indicators. Because of low density of the helium inside the high-altitude balloon, the shape of the balloon on the ground is an inverted cone, which means the stress of the envelope material is non-uniform. The numerical simulation of the high-altitude balloon under two different wind conditions is carried out in this paper. Fig. 7 and Fig. 8 show the simulation results of the high-altitude balloon under the ground wind speed of 2 m/s and 4 m/s, respectively. As shown in Fig. 7(c) and Fig. 8(c), the pressure distribution of the balloon presents obvious lateral and vertical inhomogeneity which leads to the local stress concentration on the episphere of the balloon. As shown in Fig. 7(a) and Fig. 8(a), the envelope material under the tensile rope of the balloon should be partly strengthened and the safety factor can be brought down in other parts of the envelope material. It also can be seen that the balloon leans more sharply, and deformation becomes larger under the action of tension and wind load with

the increase of wind speed, which are basically consistent with the real situation. The proposed constitutive relation in this paper can effectively predict the mechanical properties and can provide some guidance to structure design of the SSA.

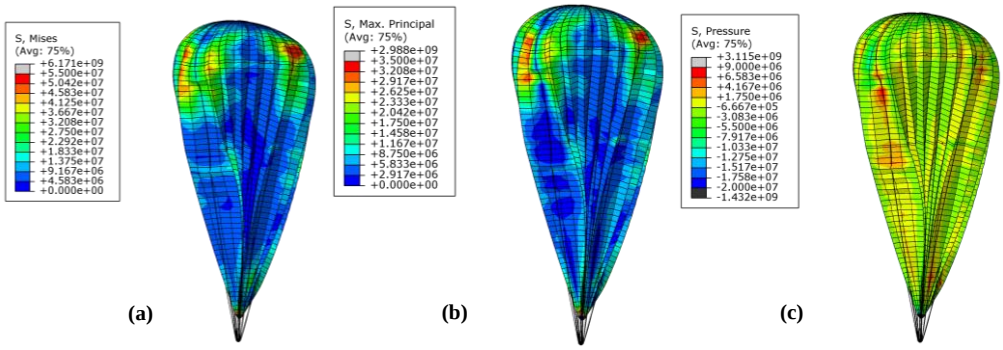

Figure 7: (a) The Von Mises stress (b) the maximum main stress and (c) pressure distribution of the SSA under the ground wind speed of 2m/s

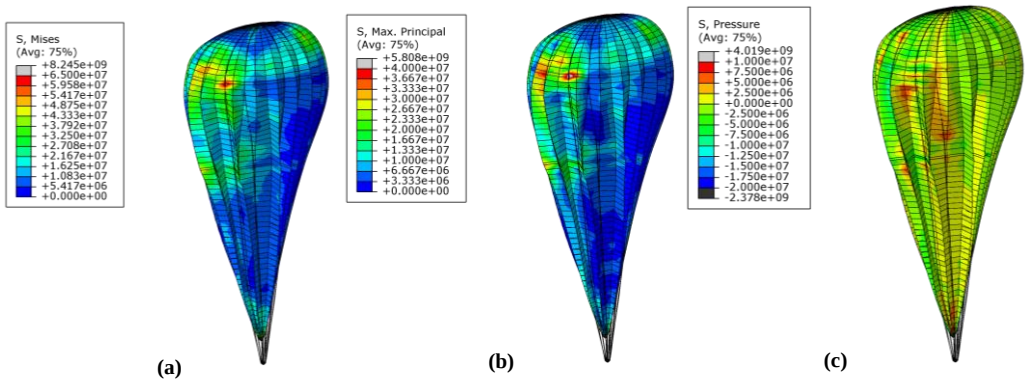

Figure 8: (a) The Von Mises stress (b) the maximum main stress and (c) pressure distribution of the SSA under the ground wind speed of 4m/s

6 Conclusions

In this study, the constitutive relation of the envelope material of a stratospheric airship, which is a fabric membrane composite, was investigated based on invariant theory. The mesoscopic deformation mechanism of the envelope material was studied first, which can be divided into before and after locking angle stages. In the first stage, the viscosity of resin matrix and friction of yarns are motived at the same time to overcome the external load. After the locking angle, waft and weft yarns contact and squeeze with each other, which means the extrusion force is added to resist the external load. According to the moment equilibrium, the Helmholtz free-energy function of system can be expressed by twenty-eight invariants, which can be transformed by five different variables. The five different variables signify the viscosity and elasticity of the fiber and matrix and

directional properties of the yarns. The constitutive equation can be derived and simplified by the on-axial and off-axial tensile tests. The results showed that the numerical calculation basically agrees with the tensile tests, and the theoretical model has a high degree of precision. At last, numerical simulation of a high-altitude balloon with a diameter of 40m flying at the stratosphere was carried out that applied the proposed constitutive relation. The results confirmed that it can reflect mechanical properties of the envelope material accurately.

Acknowledgment: This work was supported by the China Postdoctoral Science Foundation under Grant No. 2016M600891. The authors thank all the people involved in the past and present progress of the experiment. The authors also are grateful to the reviewer and the executive editor for their precious suggestions about this paper.

References

Ambroziak, A.; Kłosowski, P. (2014): Mechanical properties for preliminary design of structures made from PVC coated fabric. *Construction and Building Materials*, vol. 50, pp. 74-81. DOI:10.1016/j.conbuildmat. 2013.08.060.

Ambroziak, A. (2005): Analysis of non-linear elastic material properties of PVC-coated Panama fabric. *Task Quarterly*, vol.9, no.2, pp.167-178.

Argyris, J.; Doltsinis, I. S. (1991): Constitutive modelling and computation of non-linear viscoelastic solids. Part I: Rheological models and numerical integration techniques. *Computer Methods in Applied Mechanics and Engineering*, vol.88, no.2, pp. 135-163.

Bonet, J.; Burton, A. (1998): A simple orthotropic, transversely isotropic hyperelastic constitutive equation for large strain computations. *Computer Methods in Applied Mechanics and Engineering*, vol.162, no.1, pp.151-164.

Chen, S.; Ding, X.; Fangueiro, R.; Yi, H.; Ni, J. (2008): Tensile behavior of PVC-coated woven membrane materials under uni- and bi-axial loads. *Journal of Applied Polymer Science*, vol.107, no.3, pp.2038-2044. DOI:10.1002/app.27303.

Holzapfel, G. A.; Gasser, T. C. (2001): A viscoelastic model for fiber-reinforced composites at finite strains: Continuum basis, computational aspects and applications. *Computer Methods in Applied Mechanics and Engineering*, vol.190, no.34, pp. 4379-4403. DOI: http://dx.doi.org/10.1016/S0045-7825(00)00323-6.

Inamoto, Y.; Saito, K.; Shibasaki, K.; Sasa, S.; Kohno, T.; Harada, K. (2003): Flight control testing for the development of stratospheric platform airships. *AIAA's 3rd Aviation Technology, Integration, and Operations (ATIO) Conferences*, Denver, USA

Jamison, L.; Sommer, G. S.; Porche III, I. R. (2005): High-altitude airships for the future force army. *DTIC Document*.

Jiang, Y.; Tabiei, A.; Simitses, G. J. (2000): A novel micromechanics-based approach to the derivation of constitutive equations for local/global analysis of a plain-weave fabric composite. *Composites Science and Technology*, vol.60, no.9, pp.1825-1833.

Khoury, G. A. (2012): *Airship technology.* vol.10, Cambridge university press.

Kyriacou, S.; Humphrey, J.; Schwab, C. (1996): Finite element analysis of nonlinear orthotropic hyperelastic membranes. *Computational Mechanics*, vol.18, no.4, pp. 269-278.

Kłosowski, P.; Zagubień, A.; Woznica, K. (2004): Investigation on rheological properties of technical fabric "Panama". *Archive of Applied Mechanics*, vol.73, no.9-10, pp.661-681.

Lee, Y.-G.; Kim, D.-M.; Yeom, C.-H. (2006): Development of Korean high-altitude platform systems. *International Journal of Wireless Information Networks*, vol.13, no.1, pp.31-42.

Luo, S.-Y.; Chou, T.-W. (1988): Finite deformation and nonlinear elastic behavior of flexible composites. *Journal of Applied Mechanics*, vol.55, no.1, pp.149-155.

Meng, J.; Li, P.; Ma, G.; Du, H.; Lv, M. (2016): Tearing Behaviors of Flexible Fiber-Reinforced Composites for the Stratospheric Airship Envelope. *Applied Composite Materials*, pp.1-15.

Nayfeh, A. H.; Kress, G. (1997): Non-linear constitutive model for plain-weave composites. *Composites Part B: Engineering*, vol.28, no.5, pp. 627-634.

Nedjar, B. (2007): An anisotropic viscoelastic fibre–matrix model at finite strains: continuum formulation and computational aspects. *Computer Methods in Applied Mechanics and Engineering*, vol.196, no.9, pp.1745-1756.

Roney, J. A. (2007): Statistical wind analysis for near-space applications. *Journal of Atmospheric and Solar-Terrestrial Physics*, vol.69, no.13, pp.1485-1501.

Smith, M.; Rainwater, L. (2003): Applications of scientific ballooning technology to high-altitude airships. *AIAA's 3rd Annual Aviation Technology, Integration, and Operations (ATIO) Technology Conference*. pp.17-19.

Weiss, J.A.; Maker, B. N.; Govindjee, S. (1996): Finite element implementation of incompressible, transversely isotropic hyperelasticity. *Computer Methods in Applied Mechanics and Engineering*, vol.135, no.1, pp.107-128.

Yingying, Z.; Xiaoguang, S.; Qilin, Z.; Henglin, L. (2014): Fracture failure analysis and strength criterion for PTFE-coated woven fabrics. *Journal of Composite Materials*, vol.49, no.12, pp. 1409-1421. DOI:10.1177/0021998314534706.

Yousef, M. I.; Stylios, G. K. (2014): Legacy of the Zeppelins: defining fabrics as engineering materials. *The Journal of The Textile Institute*, vol.106, no.5, pp. 480-489. DOI:10.1080/00405000.2014.926606.

Zheng, Z.; Huo, W. (2013): Planar path following control for stratospheric airship. *IET Control Theory & Applications*, vol.7, no.2, pp. 185-201. DOI: 10.1049/ iet-cta. 2011. 0 462.

Zheng, Z.; Zhu, M.; Shi, D.; Wu, Z. (2014): Hovering control for a stratospheric airship in unknown wind. DOI:10.2514/6.2014-0973.